PROCEEDINGS OF SCIENCE

Exploration of the physical origin of blazar flares with a time-dependent one-zone model

Paloma Thevenet
LUTH, Observatoire de Paris, CNRS, PSL, Univ. Paris Cité; 5 Pl. Jules Janssen, 92195 Meudon, France
E-mail: paloma.thevenet@obspm.fr

Andreas Zech
LUTH, Observatoire de Paris, CNRS, PSL, Univ. Paris Cité; 5 Pl. Jules Janssen, 92195 Meudon, France
E-mail: andreas.zech@obspm.fr

Catherine Boisson
LUTH, Observatoire de Paris, CNRS, PSL, Univ. Paris Cité; 5 Pl. Jules Janssen, 92195 Meudon, France
E-mail: catherine.boisson@obspm.fr

Multi-wavelength flux variability is a well-known signature of emission from active galactic nuclei and in particular from blazars. Rapid flares, with variability of the order of a few days and below, are frequently observed at high energies from these objects. While many physical interpretations have been proposed for individual flare events, based on radiative models with varying degrees of complexity, a general picture of their physical origin is still lacking.
Here we focus on a description of rapid flares as isolated events, for which a description based on a single compact emission region is appropriate. We have explored the parameter space of a one-zone synchrotron self-Compton model for different scenarios leading to flares due to temporary perturbations of a steady state. Such perturbations can be based on additional particle injection, diffusive shock acceleration, or stochastic acceleration on turbulence. The time-dependent EMBLEM code has been used to solve the kinetic equation describing the evolution of the electron distribution, simulate broad-band spectral distributions and multi-wavelength light curves.
We have identified observable signatures in the shape of the resulting light curves and in the relative amplitudes between different bands to distinguish between these generic scenarios.

High Energy Phenomena in Relativistic Outflows VIII - HEPRO VIII
October 2023
Institut d'Astrophysique de Paris, France

PoS(HEPROVIII)080

1. Introduction

Blazars are active galactic nuclei (AGN) presenting two beamed relativistic jets, seen from the Earth with a line of sight directed very close to the jet axis. The synchrotron emission, from the radio band to UV or X-rays, and the inverse Compton (IC) emission, at higher energies, lead to a very distinguishable broad-band spectral energy distribution (SED) presenting a two-bump structure: the first bump results from the synchrotron radiation of high-energy electrons and the second bump, in what is the most common view, from the IC scattering of soft photons. In the case of BL Lac type blazars, which we restricted our study to, the dominant soft photon field in the emission region is the radiation resulting from the synchrotron emission itself, leading to a synchrotron self-Compton (SSC) scenario [1] [2].

One of the main characteristics of blazars is their high variability. One observes peaks of increased luminosity over all energy bands, from the radio band to VHE γ-rays. Flares typically occur over timescales of a few days down to the minute scale at high energies, while in the radio band the variations are slower (months to years). Numerous individual flares have been studied using radiative models, but we still lack a broader picture of their physical origin. To reproduce blazar variability and to better understand the mechanisms leading to the observed flares, we model the evolution of the particle population with a blob-in-jet model. In this work we consider events of short duration, constraining the emission region to a compact zone due to causality arguments. We therefore apply a one-zone model and we also limit this first study to a purely leptonic scenario.

To simulate blazar flares, we used the EMBLEM (Evolutionary Modeling of BLob EMission) code, developed by [3]. We simulated several flaring scenarios described in section 3 and found recognizable patterns that can help to characterize observations. We studied flares resulting from simple additional particle injection in the blob and implemented the possible adiabatic expansion of the emission zone to study its effect, in the case of a moving plasma blob in an open jet. We also studied flaring events resulting from the acceleration of particles inside the blob, by Fermi II and Fermi I acceleration [4].

2. Analytical model

We consider a spherical blob of radius $R(t)$, Doppler factor δ, redshift z, carrying a tangled magnetic field $B(t)$ and an evolving electron population. The blob may be expanding adiabatically over a timescale t_{ad}. To account for the steady emission in the absence of flares, we assume a source of continuous particle injection $Q_{inj}(\gamma,t)$. Broad-band continuous emission from (a) more extended region(s) may add to this, but this is ignored here. During flares, the quiescent injection can be topped by a time-dependent one, which may have a harder electron distribution. In addition, the particles in the blob can be accelerated by two mechanisms: stochastic (Fermi II) acceleration and diffusive shock acceleration (DSA) (Fermi I). These are respectively characterized by the time-dependent acceleration timescale $t_{F_{II}}(t)$ and the time-independent acceleration timescale t_{shock}. The electrons moreover lose energy by emitting synchrotron and IC radiation. Finally, the particles can escape the blob within a timescale t_{esc}, independent of time and energy unless turbulence is present. In the latter case we denote the escape timescale $t_{esc}^{(turb)}(\gamma,t)$. The evolution of the electron distribution $N_e(\gamma,t)$ within the blob, taking into account the above processes, is governed by the

following Fokker-Planck equation [5], [6]:

$$\frac{\partial N_e(\gamma,t)}{\partial t} = \frac{\partial}{\partial \gamma}\left[\left(b_c(\gamma,t)\gamma^2 + \frac{1}{t_{ad}}\gamma - a(t)\gamma - \frac{2}{\gamma}D_{F_{II}}(\gamma,t)\right)N_e(\gamma,t)\right] + \frac{\partial}{\partial \gamma}\left(D_{F_{II}}(\gamma,t)\frac{\partial N_e(\gamma,t)}{\partial \gamma}\right) - N_e(\gamma,t)\left(\frac{1}{t_{esc}} + \frac{3}{t_{ad}}\right) + Q_{inj}(\gamma,t) \tag{2.1}$$

This kinetic equation is driven by injection, cooling and acceleration terms:

- Injection
  The last term in the right-hand-side (r.h.s) of equation 2.1 accounts for particle injection, which follows a broken power law with an exponential cutoff.

- Cooling

  1. Radiative cooling: the total cooling rate $b_c(\gamma,t)$ takes into account both the synchrotron and IC cooling [7, 8]. The full Klein-Nishina cross-section is evaluated for IC cooling.

  2. Adiabatic expansion: the expansion affects the electron energy distribution in two manners [9]. First, the relativistic electrons lose energy at a rate $1/t_{ad}$ as they behave kinematically like photons. Second, the change in volume of the blob leads to a direct change of the electron spectrum $N_e(\gamma,t)$ because of the decrease in particle density during the expansion, expressed by the term $-3N_e(\gamma,t)/t_{ad}$. The adiabatic cooling timescale is $t_{ad}(t) = R(t)/(\beta_{exp}c)$. The expansion speed β_{exp} depends on the intrinsic opening angle of the jet α: $\beta_{exp} = \beta_{jet}\tan(\alpha)$. We assume $\alpha = \rho/\Gamma$ where ρ is a parameter found to be 0.26 rad as best-fit value based on radio VLBI observations [10]. The presence of adiabatic expansion also implies an evolving blob radius and magnetic field, which we treat as in [11]. We denote the initial values before expansion by R_0 and B_0[1].

  3. Escape: the escape timescale t_{esc} is a constant value when studying flares resulting from particle injection only, while in the case of turbulence, it can depend on time and energy. In the specific case of 'hard-sphere' scattering that we restrict our study to, the escape timescale is dependent of time but independent of the electrons' energy [6]:

$$t_{esc}^{(hard)} = \left(\frac{R}{c}\right)^2\left(\frac{\delta B}{B}\right)^2\frac{c}{\lambda_{max}} \tag{2.2}$$

  with the turbulence level $\delta B/B$ and longest wavelength in the Alfvén spectrum λ_{max}.

- Acceleration

  1. Fermi II: We follow the usual description of stochastic particle acceleration on MHD waves. The fourth r.h.s term corresponds to the drift of electrons to higher Lorentz factor due to stochastic acceleration, with the diffusion coefficient $D_{F_{II}}(\gamma,t) = p^2/t_{F_{II}}$ where $t_{F_{II}}$ is the Fermi II acceleration timescale and p is the electron momentum. The acceleration timescale is, in the case of

[1] In this study the escape timescale is kept constant in the case of adiabatic expansion: $t_{esc} = 1R_0/c$. It is updated to vary as $t_{esc} = 1R(t)/c$ in a forthcoming publication; the effects of the blob expansion on the LCs remain qualitatively the same.

hard-sphere scattering:

$$t_{F_{II}}^{(hard)} = \frac{1}{\beta_A^2}\left(\frac{B}{\delta B}\right)^2 \frac{\lambda_{max}}{c} \tag{2.3}$$

with β_A the time-dependent Alfvén speed, that varies between typical orders of magnitude $10^{-2} - 10^{-1}$c. This stochastic acceleration also leads to the diffusion of the electron distribution with the Lorentz factor which is described by the fifth term of second derivative in γ.

2. Fermi I: in this preliminary study, the systematic energy gain of particles is approximated with the term $a(t) = 1/t_{shock}$ where t_{shock} is the constant acceleration timescale.

The original EMBLEM code has been modified to include a full description of adiabatic expansion and cooling, and to allow for time-dependent escape and acceleration time scales in the case of stochastic acceleration.

3. Flare scenarios

The jet and (initial) blob parameters are the same for the different flare scenarios and are based on the study of the source Mrk 421 by [3], assuming in particular $R_0 = 3e16$ cm, $B_0 = 0.04$ G, $\delta = 29$. We know that, given the typical SED of this hard-spectrum source, IC emission occurs in the Klein-Nishina regime. The flaring phase lasts for a duration $t_{dur} = 3$ observer days ≈ 8 R/c. Except during the flaring phase when there is turbulence, the escape timescale is fixed at $t_{esc} = 1$ R/c.

- Particle injection: the flaring corresponds to an additional steady particle injection in the blob during t_{dur} with a harder spectrum. The spectrum slope is -2.23 for the quiescent injection and -1.6 during the flaring phase in order to mimic the injection of freshly accelerated particles into the blob. There is no acceleration, no blob expansion.

- Injection and adiabatic expansion: the same flaring scenario as for simple particle injection, but including adiabatic expansion of the blob for an intrinsic opening angle $\alpha \approx 0.44°$, corresponding to the chosen Doppler factor, while assuming a viewing angle of $\theta = 1°$.

- Fermi II acceleration: the flaring corresponds to the stochastic acceleration of blob particles during t_{dur}, with time-dependent escape timescale $t_{esc}^{(turb)}$. We vary the turbulence level $0 < \delta B/B \leq 1$ and maximum wavelength $0 < \lambda_{max} \leq R$ to explore the impact of different acceleration time scales. There is no additional particle injection, no blob expansion.
  For this scenario, we present three models corresponding to different acceleration efficiencies that lead to different levels of Compton dominance (CD), defined as the ratio of the energy flux at the IC peak to the energy flux at the synchrotron peak.

  1. Low CD: we set $\delta B/B = 1$ and $\lambda_{max} = 1$ R for an initial acceleration time $t_{F_{II}}^0 \approx 15$ R/c.
  2. Intermediate CD: we set $\delta B/B = 0.5$ and $\lambda_{max} = 0.14$ R for $t_{F_{II}}^0 \approx 6$ R/c.
  3. High CD: we set $\delta B/B = 1$ and $\lambda_{max} = 0.14$ R for $t_{F_{II}}^0 \approx 2$ R/c.

- Fermi I acceleration: the flaring corresponds to DSA during t_{dur} of timescale $t_{shock} = 1.3$ R/c. This acceleration dominates the underlying stochastic acceleration of parameters $\delta B/B = 1$ and $\lambda_{max} = 1$. There is no additional particle injection, no blob expansion.

4. Resulting light curves

For each scenario we calculate the time-dependent electron distribution and corresponding SED. The light curves (LC) are obtained by integration the SED over time in the corresponding energy ranges, shown by the coloured bands in Figure 1: 100 - 3000 GHz = $4 \cdot 10^{-4}$ - 10^{-2} eV for the radio, 3.5 $-$ 1.5 eV for the optical, $2 \cdot 10^{2}$ - 10^{4} eV for the X-rays, 10^{8} - 10^{11} eV for the γ-rays and $2 \cdot 10^{11}$ - 10^{14} eV for the VHE γ-rays.

An example of a time-dependent SED for a case of very efficient stochastic acceleration is shown in Figure 1. After an initial large increase in the flux and an increased CD, IC cooling is shifting the peaks to lower frequencies.

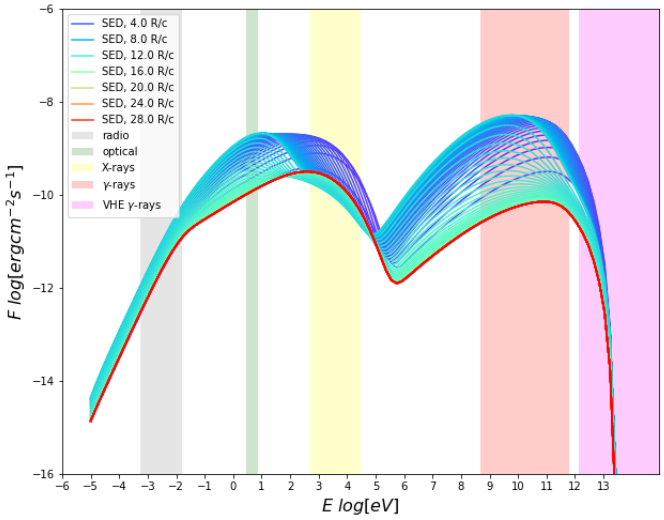

Figure 1: SED obtained for the case of intermediate Fermi II acceleration. The colored curves (purple - blue - green - red) represent the temporal evolution during the entire simulation. The first timestep is identical to the final one, hence covered by the red curve. The vertical bands correspond to the area integrated to compute the LCs in five energy bands: radio (gray), optical (green), X-rays (yellow), γ-rays (red) and VHE γ-rays (purple).

We present in Figure 2 a comparison of LCs for the different scenarios, limiting Fermi II to the intermediate CD case. To be able to compare the curves, we have tried to choose parameters that lead to similar flux amplitudes in the X-ray band. A comparison of LCs for the low, intermediate and high CD Fermi II scenarios are shown in Figure 3.

For flares caused by additional particle injection, the LC rise is always concave. For a sufficiently low rate of the additional injection, the asymmetry of the flare profile is positive, i.e. the rise-time is longer than the decay time. The CD remains inferior or similar to 1. The escape timescale of electrons determines the relative variability amplitude between X-ray and γ-ray/VHE γ-ray domains. Including the adiabatic expansion leads to a decreasing quiescent emission and decreasing plateau (when reached) and to a negative asymmetry.

Flares induced by stochastic acceleration of low and intermediate CD type, i.e. with CD less than

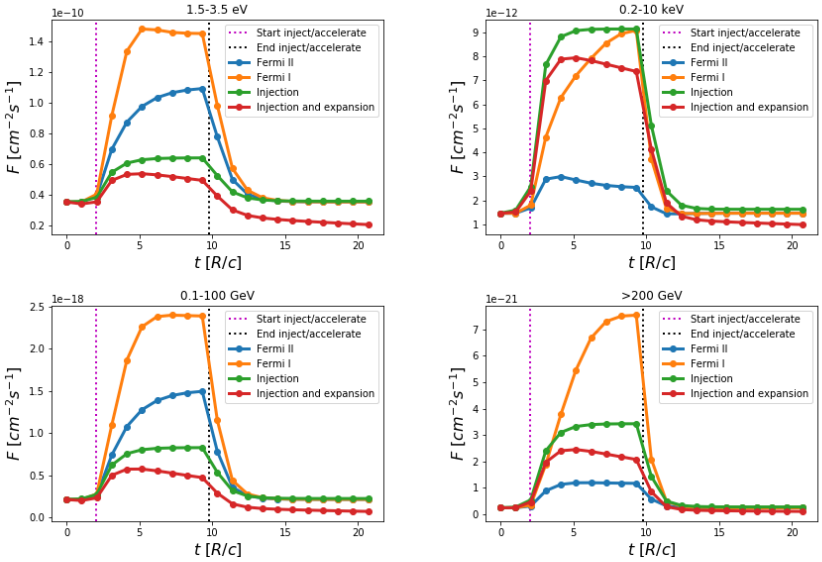

Figure 2: LCs comparison of five different flaring types. The flux evolution is given in the optical band (top left), X-ray band (top right), γ-ray band (bottom left) and VHE γ-ray band (bottom right). The Fermi II acceleration scenario is implemented for the intermediate CD regime.

or approximately 1, present a concave rise and positive asymmetry. These flares have a larger variability amplitude (VA) in the radio, optical and HE γ-ray bands compared to flares resulting from particle injection. The acceleration is not sufficiently efficient in this regime to achieve an X-ray flux comparable to the other scenarios.

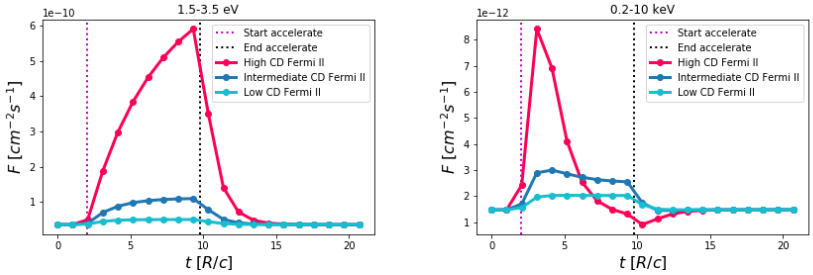

Figure 3: LC comparison of three different Fermi II acceleration timescales corresponding to the low, intermediate and high CD regimes, in the optical (left) and X-ray band (right).

High CD Fermi II flares have a concave/linear rise in the radio, optical and γ-ray bands, while it is convex in the X-rays and VHE γ-rays. The CD is larger than 1 and the VA of the (V)HE γ-ray bands is larger by 1-2 orders of magnitude compared to the other domains. The flare rise is fast, so the asymmetry is negative, and the decay takes place early in the X-rays and VHE γ-rays (before the end of the acceleration phase).

Flares resulting from DSA have a larger VA in the (V)HE γ-ray bands compared to the other domains and relative to the other flaring scenarios. The plateau phase is reached at different times for different energy bands and the SED synchrotron and SSC bumps shift to higher frequencies during the flaring phase.

In all the scenarios, the escape timescale t_{esc} and the effect of radiative cooling determine the decay time and decay shapes of the flares between energy bands. The occurrence of a plateau and the asymmetry of the flares depend on the flare duration.

5. Conclusions and outlook

- Even in the absence of external photon fields, high CD can be achieved during flares induced by efficient stochastic acceleration. The times of the flare peaks can be markedly shifted between different energy bands in this case.
- Detectable differences appear in the one-zone model between flare shapes that arise from injection, stochastic or diffusive shock acceleration.
- For each scenario, when comparing different energy bands, the relative VAs and the times at which a plateau is reached are the most distinguishable features to identify the specific scenario.
- We plan to conduct a systematic study of the scenarios we have explored here. This will include a new treatment of DSA flares, implemented using a time-dependent power-law to mimic a shock front injecting additionally accelerated particles in the blob.

References

[1] L. Maraschi, G. Ghisellini and A. Celotti, *A jet model for the gamma-ray emitting blazar 3C 279*, *Astrophys. J.* **397** (1992) L5.

[2] S.D. Bloom and A.P. Marscher, *An analysis of the synchrotron self-compton model for the multiwave band spectra of blazars*, *Astrophys. J.* **461** (1996) 657.

[3] A. Dmytriiev, H. Sol and A. Zech, *Connecting steady emission and very high energy flaring states in blazars: the case of Mrk421*, *Monthly Notices of the Royal Astronomical Society* **505** (2021) 2712.

[4] J.H. Matthews, A.R. Bell and K.M. Blundell, *Particle acceleration in astrophysical jets*, *New Astronomy Reviews* **89** (2020) 101543.

[5] N.S. Kardashev, *Nonstationariness of spectra of young sources of nonthermal radio emission*, *Soviet Astronomy* **6** (1962) .

[6] A. Tramacere, E. Massaro and A.M. Taylor, *Stochastic acceleration and the evolution of spectral distributions in synchro-self-compton sources: A self-consistent modeling of blazars' flares*, *Astrophys. J.* **739** (2011) 66.

[7] M. Chiaberge and G. Ghisellini, *Rapid variability in the synchrotron self Compton model for blazars*, *Mon. Not. Roy. Astron. Soc.* **306** (1999) 551.

[8] R. Moderski, M. Sikora, P.S. Coppi and F.A. Aharonian, *Klein-Nishina effects in the spectra of non-thermal sources immersed in external radiation fields*, .

[9] R.J. Gould, *Energy loss of relativistic electrons and positrons traversing cosmic matter*, *The Astrophysical Journal* **196** (1975) 689.

[10] A.B. Pushkarev, Y.Y. Kovalev, M.L. Lister and T. Savolainen, *Jet opening angles and gamma-ray brightness of AGN*, *Astron. Astrophys.* **507** (2009) L33.

[11] A. Tramacere, V. Sliusar, R. Walter, J. Jurysek and M. Balbo, *Radio-γ-ray response in blazars as a signature of adiabatic blob expansion*, *Astron. Astrophys.* **658** (2022) A173.